Journal of lightwave Technology, Available online July
DOI:10.1109/JLT.2024.3429136

Fabrication of Hi-Bi multi-core silica optical fibre preforms from dual-curing resins incorporating nano composites

Jiaying Wang, Qingqin Han, Jing Kong, Guanghao Li, Edmond Chehura, Ralph P. Tatam, Yushi Chu, Yanhua Luo, Jianzhong Zhang, and Gang-Ding Peng

***Abstract*—Additive manufacturing (AM) or three-dimensional (3D) printing stands out for its remarkable ability to manufacture custom-designed preforms for specialty silica optical fibres (SOFs) featuring sophisticated structures and diverse material compositions. Here, a novel scheme for manufacturing preforms for highly birefringent multi-core silica optical fibres (Hi-Bi MC SOFs) is proposed and tested using specially formulated dual-curing resins with AM technologies. These resins, incorporating nano composites (NCs), are ultraviolet (UV) and thermally cured to form fibre preforms in respective AM processes. Sample silica fibre preforms are successfully fabricated with holey cladding (Ti-doped, UV cured), multiple cores (Ge-Ti co-doped, thermally cured) and stress applying parts (SAPs, B-Al co-doped, thermally cured). As confirmed by X-ray diffraction (XRD) tests, these preforms can be consolidated into clear amorphous silica with the required structure and strength, demonstrating the potential of the proposed scheme in developing preforms for specialty fibres with custom-designed structures and materials required for sensing applications.**

***Index Terms*—Optical nanomaterials, additive manufacturing, 3D printing, silica fibre preforms, highly birefringent fibres, multi-core fibres.**

This work was supported in part by the Australian Research Council under Grant LE0883038, LE100100098, in part by the UNSW Materials and Manufacturing Futures Institute under Grant PS64082-SHIR3, and in part by the Engineering and Physical Sciences Research Council, UK under Grant EP/H02252X/1, in part by the State Key Laboratory of Advanced Optical Communication Systems and Networks (Shanghai Jiaotong University, 2023GZKF022), the Science and Technology Commission of Shanghai Municipality (SKLSFO2022-01), and 111 Project (D20031).

J. Wang, Q. Han, J. Kong, G. Li, G.-D. Peng are with the Photonics and Optical Communications, School of Electrical Engineering & Telecommunications, UNSW Sydney, NSW 2052, Australia and the Materials and Manufacturing Futures Institute, UNSW Sydney, NSW 2052, Australia (e-mail: jiaying.wang@unsw.edu.au; qingqin.han@unsw.edu.au; jing.kong@unsw.edu.au; guanghao.li@student.unsw.edu.au; g.peng@unsw.edu.au).

E. Chehura and R. P. Tatam are with Centre for the Engineering Photonics, Cranfield University, Cranfield, Bedfordshire, MK43 0AL, UK (e-mail: e.chehura@cranfield.ac.uk; r.p.tatam@cranfield.ac.uk).

Y. Chu and J. Zhang are with the Key Laboratory of In-fiber Integrated Optics of Ministry of Education, College of Physics and Optoelectronic Engineering, Harbin Engineering University, Harbin 150001, China and Yantai Research Institute & Graduate School, Harbin Engineering University, Yantai 264000, China (e-mail: chuyushi@hrbeu.edu.cn; zhangjianzhong@hrbeu.edu.cn).

Y. Luo is with the Key Laboratory of Specialty Fiber Optics and Optical Access Networks, Joint International Research Laboratory of Specialty Fiber Optics and Advanced Communication, Shanghai Institute for Advanced Communication and Data Science, Shanghai University, Shanghai 200444, China (e-mail: yhluo3@shu.edu.cn).

I. Introduction

In the rapidly advancing field of optical fibre technology, the pursuit of higher performance and greater functionality has given rise to the development of highly birefringent multi-core silica optical fibres (Hi-Bi MC SOFs) – an innovation that holds great promise for revolutionizing optical communication systems and sensor networks [1-5]. These fibres utilize silica, recognized for its low signal attenuation and excellent optical transparency, as the primary material [6]. They involve the complex integration of multiple cores within a single fibre structure, enabling various applications such as parallel data transmission, integrated photonics, sensor arrays, distributed sensing, and biomedical imaging [7-10]. Simultaneously, these fibres exhibit high birefringence, i.e., different refractive indices along two orthogonal axes, triggered by the varying thermal expansion coefficients of stress applying parts (SAPs) and cladding. This feature allows precise control and measurement of light polarization and has been widely applied in fibre optic sensors, including polarimetric sensors, polarization-based chemical sensors, fibre optic gyroscopes, as well as temperature and strain sensors [11-14]. However, conventional fabrication technologies, relying on chemical vapor deposition and rod-and-tube stacking, face challenges in fabricating Hi-Bi MC SOFs with such intricate structures, particularly when dealing with SAPs that have complex structures and materials [15, 16]. Recent developments in three-dimensional (3D) printing technology may provide solutions to address these limitations.

3D printing, also known as additive manufacturing (AM), is a rapid prototyping technology that offers remarkable material flexibility and extensive freedom in structural design. Common technologies include fused deposition modeling (FDM), selective laser sintering (SLS), digital light processing (DLP), and extrusion or casting [16-22]. The feedstock used in this study is dual-curing resins containing SOF nano composites (NCs). These resins, categorized as low-melting-point optical nanomaterials, eliminate the need for the high-temperature environment typically required in most SOF fabrications. Under the influence of ultraviolet (UV) light and thermal effects, this feedstock, loaded with various silica fibre NCs, can be cured into a series of complex shapes. In recent years, the use of dual-curing resins in 3D printing has successfully

Published by IEEE. This is the Author Accepted Manuscript issued with: Creative Commons Attribution License (CC:BY 4.0).
The final published version (version of record) is available online at DOI:10.1109/JLT.2024.3429136. Please refer to any applicable publisher terms of use.

manufactured several SOFs with special designs, including Yb-doped micro-structured fibres [23], multi-core Bi/Er co-doped fibres [24] and multi-function twin core Bi/Er co-doped fibres [25]. This makes 3D printing an ideal method for the fabrication of Hi-Bi MC SOFs.

In this paper, we proposed and tested a novel scheme using AM technologies to fabricate Hi-Bi MC SOF preforms from specially formulated UV- and thermal-curing resins that incorporate NCs. The process involves UV-curing of cladding, thermal-curing of cores and SAPs, as well as thermal processing of cured green bodies, demonstrating the successful fabrication of Hi-Bi MC SOF preforms. Sample preforms, doped with TiO_2, GeO_2, B_2O_3, and Al_2O_3 in the cladding, cores, and SAPs, have achieved the required consolidated structure and strength in the form of clear amorphous silica, as confirmed by X-ray diffraction (XRD) testing of the thermally processed preform samples.

II. Experiment Section

A. *Novel Preform Scheme for Hi-Bi MC SOFs*

The pathway we take to fabricate Hi-Bi MC SOFs involves two main steps: 1) fabricating fibre preforms under the novel AM technology scheme proposed here and 2) drawing SOFs by conventional draw-tower techniques. In this preliminary work, we will focus only on the first step since the main research challenges/problems exist in manufacturing fibre preforms.

The standard design of Hi-Bi fibres consists of three material types: cladding, core, and SAP in the structural form of bow-tie, PANDA, or elliptical jacket. In this work, we propose an AM technology-based scheme of Hi-Bi preform fabrication using dual-curing resins containing different NCs, as shown in Fig. 1.

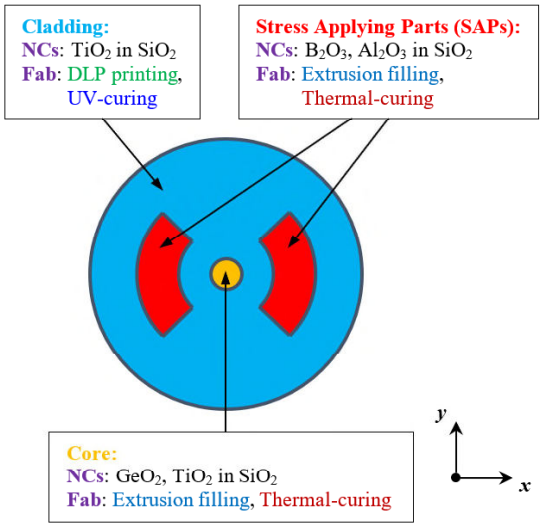


Fig. 1. Proposed Hi-Bi preform scheme using dual-curing resins incorporating different nano composites (**NCs**) and AM technology-based fabrication (**Fab**): DLP printing (UV-curing) for cladding, extrusion filling (thermal-curing) for core and SAPs. The two orthogonal axes are denoted as *x* and *y*, respectively.

To demonstrate the advantage of this new scheme, we start with relatively challenging preforms for Hi-Bi MC SOF, as demonstrated in Fig. 2(a) (3-core) and Fig. 2(b) (4-core). The claddings (Fig. 2(c)) of two types of Hi-Bi MC SOF preforms are designed using Autodesk Inventor for DLP printing. Based on the proposed scheme, these Hi-Bi MC preforms build upon three functional parts: 1) the cladding, which has a special complex structure and is printed using UV-curing DLP technology; 2) SAPs, containing materials with different thermal expansion coefficients from the cladding, produced through extrusion filling and thermal curing; 3) cores that generate birefringence, also made via thermal-curing extrusion technology. The outer cladding diameter (D) and radius (r_1 and r_2) of the SAPs are set as 24.000 mm, 3.146 mm, and 5.424 mm, respectively. They will be doped with materials having different coefficients of thermal expansion to achieve high birefringence in the fibre cores. The diameter of all cores (d) is 3.000 mm, which includes an eccentric marking core designed to differentiate the Hi-Bi cores. This design combines the abilities of multi-core and highly birefringent fibres in one package. Moreover, a set of 3.000×3.000 mm openings is introduced at the starting end of the preforms to minimize the generation of bubbles during printing, caused by the multiple hollow parts of the design structures (as illustrated in Fig. 2(c)).

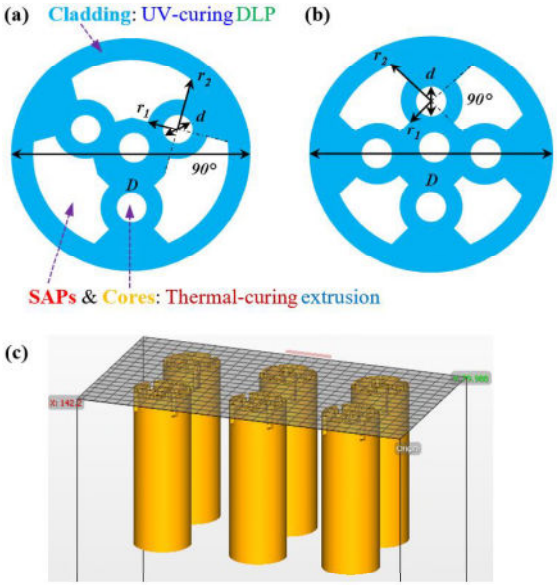


Fig. 2. Designed structures: (a) 3-core cross-section, (b) 4-core cross-section with 90° bow-tie SAPs, both featuring an eccentric marking core. Here, D, r_1, r_2, and d represent the outer cladding diameter, radius of the SAPs, and core diameter, respectively; (c) openings at the starting end of the preforms.

B. *Dual-curing Resin Formulation and Characterization*

Dual-curing resins, utilized as feedstock in both UV- and thermal-curing processes, should consider the following components: 1) solvents, referring to organics such as monomers and crosslinkers used for constructing the designed structure during printing; 2) solid dopants, which are inorganic silica fibre NCs used to form the fibre preforms; 3) additives, including photo initiators, thermal initiators, and inhibitors, which are vital for making resins UV and thermally curable. Based on our previous study [26], the organic chemicals (including solvents and additives) along with their respective ratios applied in customizing our dual-curing resins are listed in TABLE I. The customized dual-curing resins in the cladding, cores, and SAPs all contain the same organic chemicals and will achieve the functionality of Hi-Bi MC SOFs by

subsequently loading different silica fibre NCs.

TABLE I
ORGANIC CHEMICALS FOR DUAL-CURING RESINS

Chemicals	Abbr.	Function	Ratio (%)
2-Hydroxyethyl methacrylate	HEMA	Monomer	85.71 [a]
Tetra (ethylene glycol) diacrylate	TEGDA	Crosslinker	14.29 [a]
Diphenyl (2,4, 6-trimethylbenzoyl) phosphine oxide	DPO	Photo initiator	0.20 [b]
Hydroquinone	Hyd	Inhibitor	0.10 [b]
2,2'-Azobis (2-methylpropionitrile) solution	AIBN	Thermal initiator	0.25 [b]

All organic chemicals are purchased from Sigma-Aldrich, Australia and directly used without any further purification.
[a]With respect to the total solvent volume (for the liquid phase).
[b]With respect to the total resin weight.

The complex structures of the cladding parts are fabricated through UV-curing, employing DLP to print the target objects layer by layer under the irradiation of UV light. The Ti-doped silica resin, serving as the cladding material, should meet the requirements of high solid loading, encompassing all solid dopants as essential ingredients for silica fibre preform, and possess good rheological and photocuring properties. The former, i.e., a high mass ratio of the solid to the solvent, ensures high density and appropriate mechanical properties after printing, while the latter is crucial for the successful 3D printing and high resolution of silica fibre preforms using DLP technology. To better determine the properties of the resins, we measured the apparent viscosity with a viscometer (VISCO-895, Atago, Japan) and tested the photocuring properties using the material test function of a DLP printer (Pro 2, Asiga, Australia). For the thermal curing of the core and SAP components, thermal-curing extrusion technology is used, and there is no high requirement for the rheological properties of the silica resins. It is only necessary to ensure the uniform loading of functional silica fibre NCs, i.e., GeO_2 and TiO_2 in the cores, and B_2O_3 and Al_2O_3 in the SAPs. Curing can simply be achieved by heating in an oven (Labec ODWFH18, Australia). Among the inorganic materials for Hi-Bi MC SOF preforms, the main silica NC (Aerosil OX50) is purchased from Evonik in Germany, and the rest are purchased from Sigma-Aldrich in Australia.

C. *Fabrication Pathway*

The entire process of fabricating Hi-Bi MC SOFs from dual-curing resins follows the steps outlined in [20]: resin preparation, DLP printing of cladding, cores and SAPs extrusion filling, thermal processing, and fibre drawing, as shown in Fig. 3. Initially, a dual-curing resin with a solid loading of 0.8 (w/w) is formed by the stepwise and repetitive dispersion of SiO_2 and TiO_2 NCs in a mixture of the photosensitive organic chemicals listed in TABLE I. Then, the resin undergoes a photopolymerization reaction in the DLP printer by exposure to 385 nm UV light, carrying the solid NCs to print the green bodies of target fibre preforms layer by layer as the claddings. Following this, the printed cladding parts are extrusion-filled with core and SAP materials and heated for thermal curing. Subsequently, structural integrity and adequate strength in consolidated preforms for later fibre drawing are achieved through proper post-thermal curing, debinding, and sintering processes, utilizing a high-temperature muffle furnace (FTBR-17M, Furnace Technologies, Australia). The changes in distance among SOF-related NCs during the fabrication process are depicted in Insets ①~⑤. Finally, these preforms can be drawn into optical fibres in the form of amorphous/fused silica composites using a conventional fibre draw tower (Control Interface, United Kingdom). Here, our focus is on the fabrication of consolidated preforms.

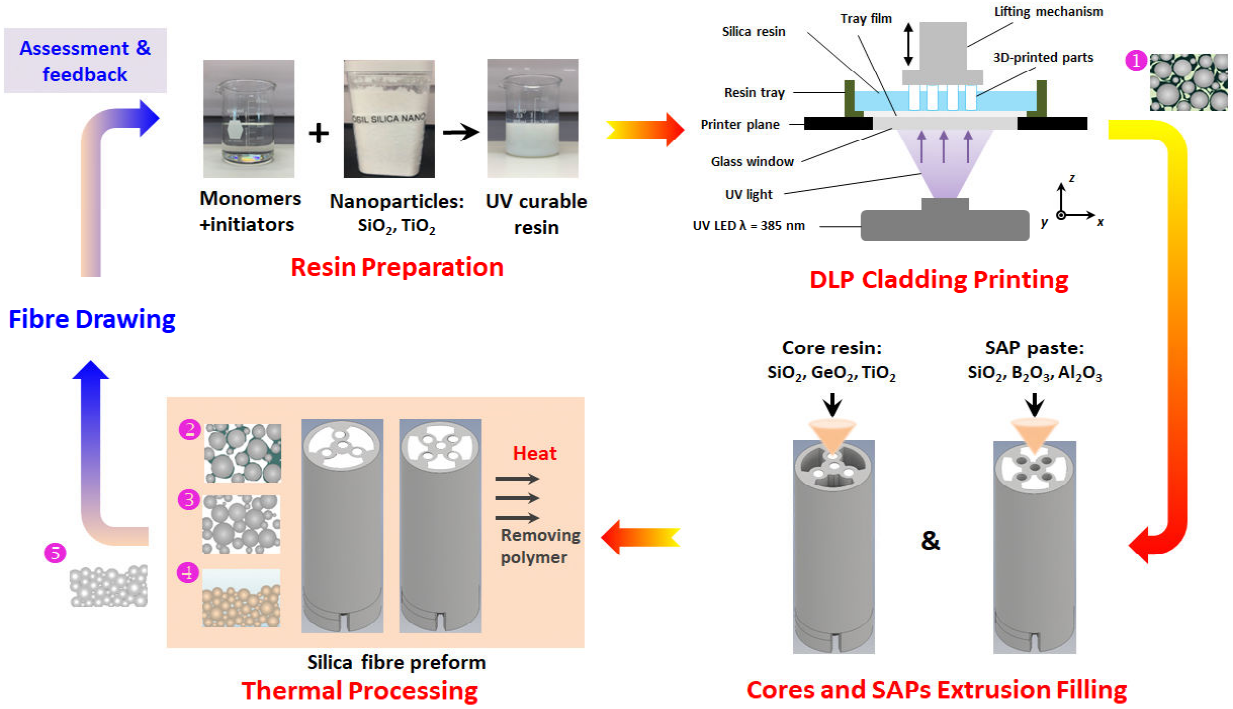


Fig. 3. Pathway of Hi-Bi MC SOF fabrication from dual-curing resins, the small pellets shown in Inserts ①~⑤ represent nano composites associated with SOFs.

III. Results and Discussion

A. Rheological and Photocuring Properties of Dual-curing Resin for DLP Cladding Printing

The resin utilized for the cladding parts in the designed fibre preforms is composed of 99.85 mol% SiO_2 and 0.15 mol% TiO_2 NCs. After appropriate settling and degassing, the 0.8 (w/w) loaded Ti-doped silica resin has a viscosity of 96.20 mPa·s at a shear rate of ~47.80 s^{-1} (using a spindle set of A1+L, rotating at 200 rpm). This viscosity is significantly lower than the maximum printing viscosity of 250.00 mPa·s for our DLP printer, indicating good rheological properties.

UV photosensitivity and photocuring resolution are two key indicators to evaluate the photocuring properties of the dual-curing resin, related to vertical growth and horizontal error, respectively. The former is used to characterize the photocuring performance and can be represented by a fitting curve between the exposure time (t) and the curing depth (C_d), expressed as [27, 28]:

$$C_d = 1/\alpha \cdot \ln(t) - C \quad (1)$$

where $1/\alpha$ represents the UV photosensitivity, that is, the slope of the vertical growth curve, and C is a constant dependent on the composition of the NCs. The photocuring accuracy is determined by the ratio of the curing depth (C_d) to the diameter sides error (ΔD), denoted as the photocuring resolution factor (R_r) and can be expressed as follows [26]:

$$R_r = C_d / \Delta D. \quad (2)$$

We adopted the same material test method as in the previous study [26] and designed a structure with an inner diameter (d) of 3.000 mm and an outer diameter (D) of 24.000 mm for photocuring testing. Fig. 4 demonstrates the corresponding curing curve and the distribution of photocuring resolution factors. The exposure time is set from 3.0 to 100.0 s with a light intensity of (I) of ~5.68 mW/cm². Additionally, photos of the cured parts at different exposure times are also presented. Observations indicate that an increase in exposure time leads to the growth of curing depth. However, the resolution factor significantly decreases with longer exposure time, especially when exceeding 10.0 s, attributed to over-curing. Moreover, the penetration of UV light decreases with increasing curing depth, causing the resulting object to take the form of a circular truncated cone rather than a standard cylinder. This outcome is also confirmed by the photos of the cured parts in Fig. 4. The undesired over-cured components extend towards both the inner diameter small hole and the outer periphery of the outer diameter as the exposure time increases, resulting in the cured parts becoming blurred.

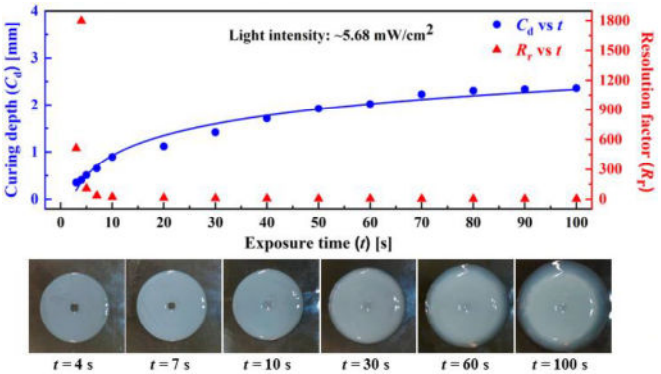


Fig. 4. Curing depth curve and distribution of photocuring resolution factors for the customized dual-curing resin, along with corresponding photos of the photocured parts at different exposure times.

To balance the curing depth and photocuring resolution factor, we selected an exposure time of 4.0 s, achieving a curing depth of 0.408 mm and the highest photocuring resolution factor of 1799.

B. DLP Printing of Cladding Parts

Derived from the photocuring test outcomes of the dual-curing resin for DLP cladding printing, the determined printing parameters include a light intensity of ~5.66 mW/cm², a slice thickness of ~0.075 mm, and an exposure time of ~4.1 s. Fig. 5 demonstrates the successful fabrication through DLP printing of Hi-Bi 3-core and 4-core fibre preforms, each with a height of ~60.000 mm and a solid loading of 0.8 (w/w). Actual print accuracy is within ~0.50 %. In the enlarged photo, it is observed that, although there is slight obscuration of the holes in the cladding parts after printing, the structures and surface finishes of the preforms become clear through a cleaning and drying process. The specific process involved carefully removing the printed parts from the platform, washing them in a 1:1 vol/vol cleaning solution of water and ethanol (Sigma-Aldrich, Australia) for ~0.5 hours, and then drying them in a fume hood for about 2 hours. At this stage, the NCs were dispersed within the organic medium and shaped into the target preforms through photopolymerization. Insert ① of Fig. 3 presents the spacing between these NCs, which have relatively large gaps filled with polymers.

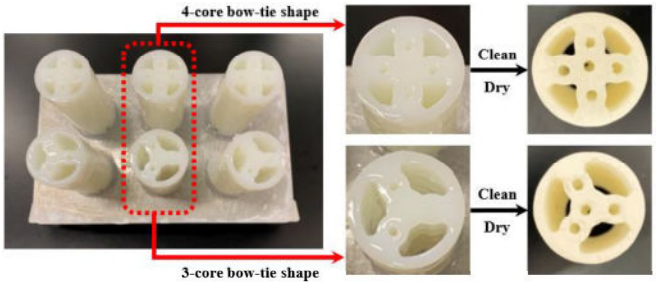


Fig. 5. Cladding parts with 3-core and 4-core bow-tie shape after DLP printing, cleaning and drying.

C. Extrusion Filling, Thermal Curing of Cores and SAPs

The dual-curing feedstock for extrusion filling consists of a 1.3 (w/w) solid-loaded SAP paste (78.62 mol% SiO_2, 19.66 mol% B_2O_3 and 1.72 mol% Al_2O_3) and a core resin (97.07 mol% SiO_2, 2.58 mol% GeO_2 and 0.35 mol% TiO_2) with a solid loading of 0.8 (w/w). Here, GeO_2 and TiO_2 are introduced into the core resin to increase the core refractive index. Al_2O_3 functions as a medium to aid the homogeneous fusion of multiple materials in the SAPs. B_2O_3 is doped into the SAP paste to achieve a thermal expansion coefficient different from that of the cladding material. This is essential for achieving high birefringence. This difference in thermal expansion coefficients, together with the particular asymmetrical geometry/location of the SAPs with respect to the core, will

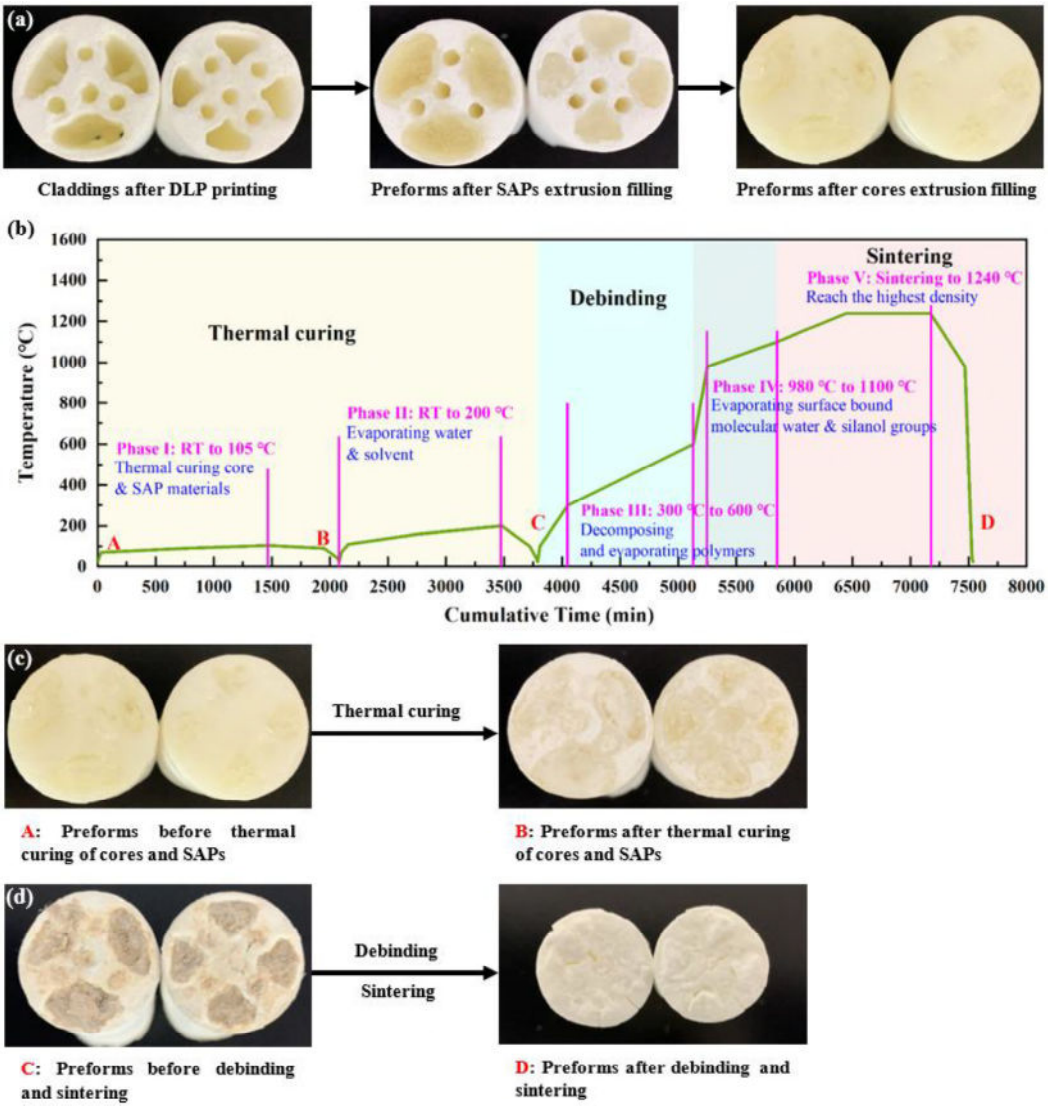


Fig. 6. Post-printing processing: (a) fibre preforms completed by extrusion filling of cores and SAPs in the printed cladding; (b) thermal processing of the completed fibre preforms; (c) the completed fibre preforms before (**A** in (b)) and after (**B**) thermal curing; (d) the cured fibre preforms before (**C**) and after (**D**) debinding and sintering.

introduce different stresses along different axes, i.e., *x* and *y*, of the core.

As illustrated in Fig. 6(a), the SAP paste was initially extrusion-filled into the cladding parts manually. The process involves extruding the solid-loaded paste into the SAP slots in the printed cladding and applying sufficient force to fill the gaps completely. The core holes are sealed in advance to prevent contamination during the filling process. Subsequently, the core resin was injected into the pre-reserved holes in the claddings using a pipette, with the bottom of the preform pre-sealed by Teflon tape. The temperature settings for thermal processing are depicted in Fig. 6(b). During the gradual temperature increase to 105 ℃ (Phase I), the filler materials were thermally cured and formed the completed preforms containing all the necessary materials for Hi-Bi MC SOFs. Corresponding photos before and after the thermal curing of cores and SAPs are also displayed in Fig. 6(c), where the integrity of the cross-section reflects the successful curing results.

D. Thermal Processing of Preforms

After DLP printing of the claddings and thermal-curing of the extruded cores and SAPs, the preforms require additional thermal processing, including post-thermal curing, debinding, and sintering, to obtain the well-consolidated final product for fibre drawing. The first step is the post-thermal curing process, which is Phase II in Fig. 6(b), during which water, solvent, and residual monomers will be evaporated. Oxidation and yellowing occur due to the presence of epoxy bonds in the epoxy structure when heated at high temperatures, resulting in a slight 'yellow' appearance of the preforms. Debinding is the second step (Phase III), where unwanted polymers in the gaps between SOF-related NCs are decomposed and evaporated (Fig. 3, Insert ②). The binders acting as supports are removed, halving the mass with little change in volume. At this point, the structure of the preforms is at its loosest and highly susceptible to fracture and cracking. In phase IV, as the temperature continues to rise to 980 ℃, surface bound molecular water and

silanol groups are removed, causing a shrinkage in the size of the preforms. This stage is also very fragile and requires a lower heating rate to maintain the integrity of the structure. Until the temperature reaches 1240 ℃ in phase V, the NCs begin to be fused together (Fig. 3, Insert ③~⑤). The size of the preforms continuously decreases, eventually reaching maximum density and completing the sintering process. Compared to the weight, height, and outer diameter of the fibre preforms before and after debinding and sintering, there is a significant reduction of approximately 44.07 %, 21.80 %, and 22.03 %, respectively. The photo on the surface of the fibre preforms in Fig. 6(d) indicates that the resulting consolidated preforms possess the required structural integrity and sufficient strength. However, at this stage, all three parts (SAP, core, and cladding) of these whitish preforms (Fig. 7(a)) do not exhibit the luster of transparent glass and are not completely vitrified. The preforms are inspected under episcopic (reflected) illumination using a polarized microscope (Eclipse LV100NPOL, Nikon, Japan) and exhibit some surface defects, as shown in Fig. 7(b).

To improve and complete the vitrification of the processed preforms, auxiliary thermal processing was conducted using a graphite furnace within the fibre draw-tower setup. These whitish preforms were first enclosed within an external commercial quartz tube and then loaded into the draw tower, where they were heated to 1760 °C for 1.5 hours under vacuum conditions of ~61 mbar. This processing resulted in fully vitrified samples with clear cross-sections, as seen in Fig. 7(c) when a sample of the Hi-Bi 4-core fibre preform is cut transversely to a thickness of ~1.44 mm. Fig. 7(d) shows the surface morphologies of the cut vitrified preform depicted in Fig. 7(c) under both episcopic (reflected) and diascopic (transmitted) illumination. These images reveal that the cladding part exhibits good transparency with a more uniform material distribution, while the SAP and core parts remain opaque and contain numerous bubbles. The presence of air bubbles is likely due to the poorer homogeneity of the filled materials and requires further research and improvement. Nevertheless, XRD tests have been carried out on the three distinct parts of the vitrified preform, and all three parts, regardless of whether they have air bubbles or not, confirmed full vitrification and a good amorphous form. As evident in the

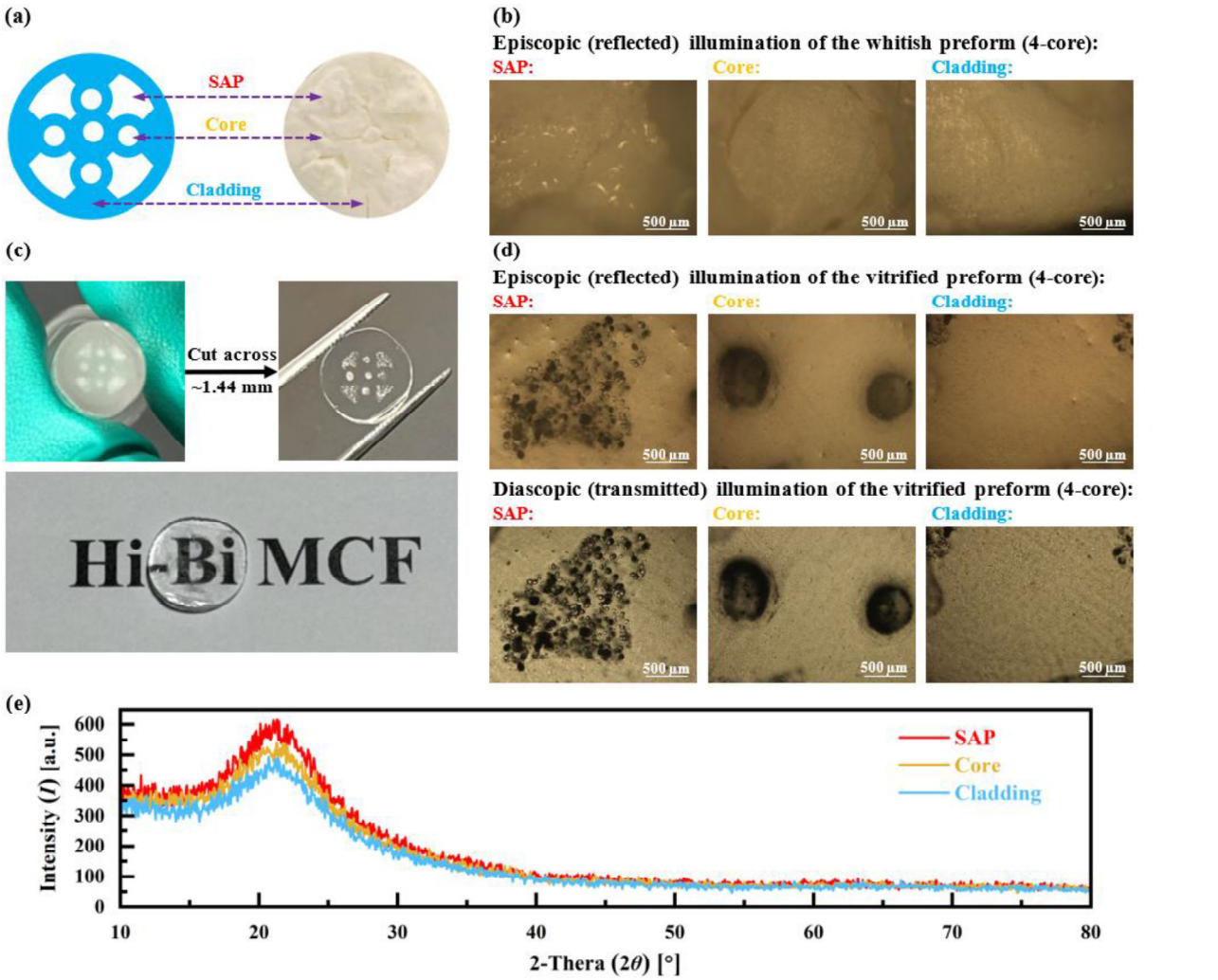


Fig. 7. Characterization of the resulting fibre preforms: (a) structural and physical diagrams of the 4-core whitish fibre preform (D in Fig. 6(d)); (b) polarized microscope images of the whitish fibre preform in (a) under episcopic illumination; (c) physical diagrams of the 4-core vitrified fibre preform; (d) polarized microscope images of the vitrified fibre preform under episcopic (top) and diascopic (bottom) illumination; (e) XRD patterns of the vitrified fibre preforms. All results include the three parts of the fibre preforms: SAP, core, and cladding.

results shown in Fig. 7(e) from XRD testing of the three parts in the sample shown in Fig. 7(c), using an X-ray diffractometer (D8 DISCOVER, Bruker, USA) with CuKα irradiation over the angular range of $10° \leq 2\theta \leq 80°$, there is no crystallization or devitrification in this vitrified preform.

IV. Conclusion

In this work, we proposed and demonstrated a novel scheme of fabricating Hi-Bi MC SOF preforms based on AM technology using UV- and thermal-curing resins incorporating NCs. Special dual-curing resins, incorporating various NCs (SiO_2, GeO_2, TiO_2, etc.) for cladding, cores, and SAPs respectively, are developed. Their rheological and photocuring properties, appropriate for UV-curing DLP technology and thermal-curing extrusion technology, are tested and confirmed. Hi-Bi MC SOF preforms are fabricated, step-by-step, by 1) DLP printing of the main structure/cladding, 2) extrusion filling of the SAPs with the paste incorporating B_2O_3 and Al_2O_3 co-doped SiO_2 NCs, 3) extrusion filling of the cores with the resin incorporating GeO_2 and TiO_2 co-doped SiO_2 NCs, and 4) thermal curing, debinding, and sintering of the whole preform green bodies. Eventually, the Hi-Bi MC SOF preforms are consolidated with the required structure and strength. Following additional vacuum high-temperature processing, these preforms are fully vitrified into an amorphous glass form, as confirmed by XRD testing. The success in designing and manufacturing these Hi-Bi MC SOF sample preforms highlights the advantage of AM-based technology over the traditional silica preform fabrication. While the quality of the final fibre preforms still needs further improvement, the progress demonstrates the promising potential of the proposed scheme for developing specialty fibre preforms with the sophisticated structures and compositions required for future sensing applications.

References

[1] J. M. Stone, F. Yu, and J. C. Knight, "Highly birefringent 98-core fiber," *Opt. Lett.*, vol. 39, no. 15, pp. 4568–4570, Aug. 2014.

[2] F. Tian, L. Yuan, Q. Dai, and Z. Liu, "Embedded multicore hollow fiber with high birefringence," *Appl. Opt.*, vol. 50, no. 33, pp. 6162–6167, Nov. 2011.

[3] Y. Kim, S. C. Warren, J. M. Stone, J. C. Knight, M. A. A. Neil, C. Paterson, C. W. Dunsby, and P. M. W. French, "Adaptive multiphoton endomicroscope incorporating a polarization-maintaining multicore optical fibre," *IEEE J. Quantum Electron.*, vol. 22, no. 3, pp. 171–178, June 2016.

[4] A. Macho, C. García-Meca, F. J. Fraile-Peláez, M. Morant, and R. Llorente, "Birefringence effects in multi-core fiber: coupled local-mode theory," *Opt. Express*, vol. 24, no. 19, pp. 21415–21434, Sept. 2016.

[5] A. M. Ortiz and R. L. Sáez, "Multi-Core Optical Fibers: Theory, Applications and Opportunities," in *Selected Topics on Optical Fiber Technologies and Applications*, InTech, 2018, pp. 63–102.

[6] H. Bach and N. Neuroth, The properties of optical glass. Springer Science & Business Media, 1998.

[7] T. Hayashi, T. Taru, O. Shimakawa, T. Sasaki, and E. Sasaoka, "Design and fabrication of ultra-low crosstalk and low-loss multi-core fiber," *Opt. Express*, vol. 19, no. 17, pp. 16576–16592, Aug. 2011.

[8] K. Nakajima, T. Matsui, K. Saito, T. Sakamoto, and N. Araki, "Multi-core fiber technology: Next generation optical communication strategy," *IEEE Commun. Mag.*, vol. 1, no. 3, pp. 38–45, Sept. 2017.

[9] F. Khan, A. Denasi, D. Barrera, J. Madrigal, S. Sales, and S. Misra, "Multi-core optical fibers with Bragg gratings as shape sensor for flexible medical instruments," *IEEE Sens. J.*, vol. 19, no. 14, pp. 5878–5884, July 2019.

[10] P. Westbrook, "Big data on the horizon from a new generation of distributed optical fiber sensors," *APL Photon.*, vol. 5, no. 2, p. 020401, Feb. 2020.

[11] M. S. Ferreira, R. M. Silva, and O. Frazão, "High-Birefringent Fiber Loop Mirror Sensors: New DevelopmentS," in *Fiber Optic Sensors*, InTech, 2012, pp. 343–358.

[12] P. Hlubina, M. Kadulova, D. Ciprian, and P. Mergo, "Temperature sensing using the spectral interference of polarization modes in a highly birefringent fiber," *Opt. Lasers Eng.*, vol. 70, pp. 51-56, July. 2015.

[13] S. Choi, S. L. Lee, J. Kim, M. S. Kim, D. K. Kim, and Y. W. Lee, "Tapered length dependence of pressure sensitivity in polarimetric fiber pressure sensor based on tapered high birefringence fiber," *IEEE Sens. J.*, vol. 20, no. 5, pp. 2492-2503, March 2020.

[14] H. Li, X. Li, D. Xu, J. Wang, and H. Yang, "Improved thermal stability of a fiber optic gyroscope using a geometric birefringence-enhanced polarization-maintaining fiber," *J. Light. Technol.*, vol. 41, no. 8, pp. 2547-2554, April 2023.

[15] J. Noda, K. Okamoto, and Y. Sasaki, "Polarization-maintaining fibers and their applications," *J. Light. Technol.*, vol. 4, no. 8, pp. 1071–1089, Aug. 1986.

[16] G.-D. Peng, Y. Luo, J. Zhang, J. Wen, Y. Chu, K. Cook, and J. Canning, "3D silica lithography for future optical fiber fabrication," in *Handbook of Optical* Fibers, G.-D. Peng, Ed. Singapore: Springer, 2019, pp. 1–17.

[17] G. D. Goh, Y. L. Yap, H. K. J. Tan, S. L. Sing, G. L. Goh, and W. Y. Yeong, "Process–structure–properties in polymer additive manufacturing via material extrusion: A review," *Crit. Rev. Solid State Mater. Sci.*, vol. 45, no. 2, pp. 113-133, 2020.

[18] Y. Luo, J. Canning, J. Zhang, and G.-D. Peng, "Toward optical fibre fabrication using 3D printing technology," *Opt. Fiber Technol.*, vol. 58, p. 102299, Sept. 2020.

[19] D. Zhang, X. Liu, and J. Qiu, "3D printing of glass by additive manufacturing techniques: a review," *Front. Optoelectron.*, vol. 14, no. 3, pp. 263–277, July 2021.

[20] J. Wang, Z. Wu, J. Kong, K. Wang, Y. Chu, Y. Luo, and G.-D. Peng, "Silica optical fibre fabrication via 3D printing technology: material processing and related issues," *Eur. Phys. J. Spec. Top.*, vol. 231, no. 4, pp. 631–642, May 2022.

[21] K. Zhang, J. Bai, X. Wan, L. Dong, S. Wang, H. Pan, Y. Chu, J. Ren, J. Zhang, and G.-D. Peng, "Facile Fabrication of Silica Glass Embedded with NiO Nanoparticles by 3D Printing Technology and its Optical Nonlinearity," *Adv. Photonics Res.*, p. 2300244, Nov. 2023.

[22] L. Dong, J. Bai, X. Wan, Z. Wu, H. Zhao, Y. Li, T. Guo, K. Zhang, J. Wang, Y. Chu, J. Zhang, and G.-D. Peng, "Effect of sintering condition on the attenuation of silica glasses fabricated by additive manufacturing," *Ceram. Int.*, vol. 49, no. 23, pp. 39400–39408, Dec. 2023.

[23] B. Zheng, J. Yang, F. Qi, J. Wang, X. Zhang, and P. Wang, "Fabrication of Yb-doped silica micro-structured optical fibers from UV-curable nano-composites and their application in temperature sensing," *J. Non Cryst. Solids*, vol. 573, p. 121129, Dec. 2021.

[24] Y. Chu, X. Fu, Y. Luo, J. Canning, J, Wang, J. Ren, J. Zhang, and G.-D. Peng, "Additive manufacturing fiber preforms for structured silica fibers with bismuth and erbium dopants," *Light Adv. Manuf.*, vol. 3, no. 2, pp. 358–364, 2022.

[25] Y. Luo, Y. Chu, X. Fu, J. Canning, J. Wang, J. Zhang, B. Yan, J. Wen, T. Wang, and G.-D. Peng, "3D printing specialty multi-function twin core Bi/Er co-doped silica optical fibres for ultra-broadband polarized near infrared emission and sensing applications," *Opt. Laser Technol.*, vol. 168, p. 109817, Jan. 2024.

[26] J. Wang, J. Kong, Q. Han, Y. Chu, Y. Luo, J. Zhang, L. Dai, and G.-D. Peng, "Surfactant effect on DLP fabrication of silica fibre preforms," *Ceram. Int.*, vol. 49, no. 10, pp. 15689–15699, May 2023.

[27] W. Lin, H. Liu, H. Huang, J. Huang, K. Ruan, Z. Lin, H. Wu, Z. Zhang, J. Chen, J. Li, Y. Ge, J. Zhong, L. Wu, and J. Liu, "Enhanced continuous liquid interface production with track-etched membrane," *Rapid Prototyp. J.*, vol. 25, no. 1, pp. 117–125, Jun. 2019.

[28] A. J. Guerra, J. Lammel-Lindemann, A. Katko, A. Kleinfehn, C. A. Rodriguez, L. H. Catalani, M. L. Becker, J. Ciurana, and D. Dean, "Optimization of photocrosslinkable resin components and 3D printing process parameters," *Acta Biomater.*, vol. 97, pp. 154-161, Oct. 2019.



https://dspace.org/

Fabrication of Hi-Bi multi-core silica optical fibre preforms from dual-curing resins incorporating nano composites

Wang, Jiaying; Han, Qingqin; Kong, Jing; Li, Guanghao; Chehura, Edmond ...

2024-09-15
Institute of Electrical and Electronics Engineers (IEEE)
https://doi.org/10.1109/JLT.2024.3429136
Wang J, Han Q, Kong J, et al., (2024) Fabrication of Hi-Bi multi-core silica optical fibre preforms from dual-curing resins incorporating nano composites. Journal of Lightwave Technology, Volume 42, Issue 18, September 2024, pp. 6547-6554

Downloaded from a DSpace repository. https://dspace.org/